Chapter 1

Experimental Techniques to Investigate Residual Stress in Joints

Roberto Montanari, Alessandra Fava and Giuseppe Barbieri

Additional information is available at the end of the chapter

http://dx.doi.org/10.5772/intechopen.71564

Abstract

Residual stress arising from welding processes is matter of great concern in industrial practice since it can affect geometry, mechanical behavior and corrosion resistance of components. In order to evaluate residual stress in welded joints and optimize post-welding heat treatments, a lot of work has been devoted to the improvement of measurement methods with increasing sensitivity and accuracy. The chapter presents and discusses some of the experimental techniques commonly used today to determine residual stress in welds and describes recent results and advancements. Destructive (sectioning, contour, hole-drilling, instrumented indentation) and nondestructive (Barkhausen noise, ultrasonic, X-ray and neutron diffraction) methods are illustrated to highlight the specific characteristics, advantages and drawbacks.

Keywords: residual stress, welding, sectioning method, contour method hole-drilling method, instrumented indentation method, Barkhausen noise method, ultrasonic method, X-ray and neutron diffraction

1. Introduction

In order to satisfy scientific and industrial needs, a lot of work has been devoted to investigate the state of residual stress in metallic materials and its effects on mechanical properties. A number of comprehensive reviews on the topic can be found in the literature (e.g. see [1–8]).

It is well known that residual stress superimposes to external applied stress and plays a crucial role in the failure of components and structures; therefore, it is taken into account in advanced design in the aerospace, automotive and nuclear fields. All manufacturing processes modify the state of stress with either positive or negative consequences; for instance, compressive surface stress increases the fatigue limit, whereas tensile residual stress may decrease the corrosion resistance.

Welding may produce huge effects on the metals: when two pieces of plates or pipes are joined together, temperature ranges from the melting point of the material to room temperature and localized high residual stress coupled with shrinkage is generated near the weld seam. After cooling to room temperature, the locked-in stress is retained leading to distortion and/or buckling. The quantitative measurement of residual stress in welded joints is of the utmost importance for the safe operation of power plants, petrochemical plants, storage tanks and transmission pipelines.

To control such effects, it is necessary to predict the macroscopic transient fields of temperature, strain and stress. In principle, this can be done by solving the equations of continuum mechanics; however, a rigorous analysis of welds is a challenging task. At the macroscopic level, a weld represents a thermo-mechanical problem of computing transient temperature, stress and strain, whereas at the microscopic level, it is a problem of physical metallurgy involving phase transformations, defect recovery, recrystallization and grain growth. Welds may consist of tens of passes, each of which contributes to the mechanical and metallurgical effects. Interactions between thermal, mechanical, metallurgical and, in the molten pool, chemical and fluid processes are quite complex, and experimental measurements are required to validate theoretical and modeling predictions.

Generally, three types of residual stress can be identified on the basis of the range over, which they are observed: the first type (σ^{I}) is termed macro-stress and influences thousands of crystalline grains; the second one (σ^{II}), the micro-stress, occurs between different phases or grains and covers a distance of about one grain; the third one (σ^{III}) ranges over few atomic distances. To study the microstructural behavior of the material, σ^{II} and σ^{III} are very important because allow for a better understanding the way in which lattice defects, in particular, dislocation arrangements, evolve. The σ^{I} stress is taken into consideration in designing engineering structures.

In many cases, the stress near the molten zone reaches the yield stress of the alloy and causes plastic deformation with microstructural changes, namely increase of point defect and dislocation density and decrease of grain size. The stresses σ^{II} and σ^{III} are strictly correlated to these microstructural features and are studied by X-ray and neutron diffraction. The techniques for analyzing σ^{II} and σ^{III} stresses involve the study of diffraction peak profiles and are not treated here because the topic goes beyond the scope of the chapter.

Several qualitative and quantitative techniques have been developed to measure residual stress. In fact, they measure strain rather than stress, and residual stress is then determined using the specific elastic constants of the material such as Young's modulus and Poisson's ratio. The wide range of available methods makes it impossible to include all of them in this chapter. In the following, some techniques, divided into two groups, namely destructive and nondestructive, will be reviewed.

The techniques of the first group are based on the destruction of the state of equilibrium of the residual stress in a mechanical component so residual stress is measured by its relaxing. The procedure used can be described as follows: (i) creation of a new stress state by machining or

layer removal; (ii) detection of the local change in stress by measuring the strain and (iii) calculation of the residual stress as a function of the measured strain through either an analytical approach or finite element (FE) calculations. The methods described here are: (i) sectioning; (ii) contour; (iii) hole-drilling and (iv) instrumented indentation.

The second group of techniques consists of nondestructive methods based on the relationship between residual stress and physical or crystallographic parameters of the material. Here, the attention has been focused on: (i) Barkhausen noise; (ii) ultrasonic; (iii) X-ray and neutron diffraction.

2. Destructive techniques

2.1. Sectioning method

The sectioning method is a destructive technique used for decades from lots of researchers to measure residual stress in structural parts and welded components. The method was developed for the first time in 1888 by Kalakoutsky to determine longitudinal stresses in a bar by slitting longitudinal strips from the bar and measuring their change in length [9, 10]. The stress analysis is simplified by assuming that transverse stress is negligible and the cutting process alone does not produce appreciable strains [8].

The slitting process is delicate since it should not introduce plasticity or heat in the cut samples maintaining the original residual stress without the influence of external factors [6]. The strains released during the cutting process are generally measured using electrical or mechanical strain gauges [6]. To determine residual stress in a plate, some attentions about sample preparation have to be done; in particular, the number of the longitudinal strips to be cut depends on the residual stress gradient [10].

The use of mechanical strain gauges have been found to be particularly suitable for the sectioning method since the device is not attached to the specimen, is not damaged during the sectioning and can be used in repeated measurements. The stress distribution over a cross section can be determined by measuring the change in length of each strip and by applying the Hooke's law [10].

The main sources of error result from temperature changes and may be practically eliminated using a reference bar of the same material.

Sectioning method has been extensively used to analyze residual stresses in welded joints, for instance, in A36 steel with fillet welds [11], high strength steel Q460 box sections [12] and thin Al-5456 panels [13]. Strips sliced at regions of high stress gradients can be considerably curved; thus, the change in length measured by the strain gauge is the change in the chord length rather than the change in arc length, which represents the actual strain [10].

In conclusion, the sectioning method is an adequate, accurate and economical technique for residual stress measurement in structural members thanks to its versatility and reliability [8, 10].

2.2. Contour method

The contour method (CM) was first proposed by Prime in 2000 [14]. CM is based on the superposition principle assuming that the material behaves elastically during the relaxation of residual stress and that the material removal introduces negligible stress [7, 14].

As shown in **Figure 1**, the displacements due to the relaxation of the internal stress are compared to an assumed flat surface contour, and the longitudinal residual stress is recreated using a FE model. The forces required to ensure that the measured deformed surface is returned to its original position are directly correlated to the residual stress. The method provides a 2D map having a regular resolution of the residual stress normal to the cut surface [14, 15].

The application of CM involves four steps: (i) cutting, (ii) measurement of surface contour, (iii) data handling and (iv) stress calculation [16].

i. *Cutting.* The cut of the sample is a crucial step since it must be precise and straight without causing plastic deformation [16, 17]; owing to its suitable characteristics, wire electric discharge machining (wire EDM) is commonly used for the purpose [18]. Special attention is required for an adequate cutting process (single flat cut, proper constraint of the specimen to avoid its movement during cutting, a constant width of cut). Moreover, the type of cutting wire, the material, the geometry of the specimen and the EDM operating parameters are extremely important to realize an optimal cut. Finally, the cutting wire should be as thin as possible to remove the minimum material, particularly in the cases where there is a high stress gradient [19].

ii. *Measuring the surface contour.* The contours of the cut surfaces can be measured using a coordinate measuring machine (CMM) [20]; typically, each surface contour is defined by about 10,000 points and the operation takes several hours.

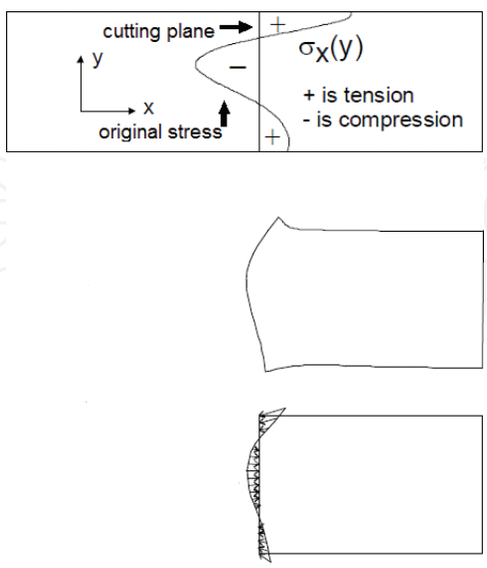

Figure 1. Schematic principles of the contour method [14].

In 2003, Prime et al. [21] developed a laser measuring system that works by moving one or more precision laser ranging probes over the entire surface with two orthogonal axes of motion, acquiring precision x, y and z spatial coordinates to submicron precision and resolution. A typical scan may take 30 min to an hour to complete with a resolution of 10 microns along the probe direction and 100 microns between scan lines. Noncontact laser surface contouring improves the capability of CM by allowing higher resolution measurement of a surface contour [21].

iii. *Data handling.* Data from the two measured surfaces are aligned. Such procedure generally requires flipping, translation and rotation of one data set to match the other. To smooth out noise in the measured surface data and to enable evaluation at arbitrary locations, the data are fitted to bivariate Fourier series. Finally, since the contour must be defined everywhere for calculating the stress, any missing area of the surface is filled in by extrapolating constant values from the defined region [16].

iv. *Stress calculation*. The residual stress is calculated from the measured surface contours using a FE model [22].

The multiaxial CM is a variation of the standard CM and its principles have been discussed by DeWald et al. [23]. This method uses displacements to calculate the eigenstrain distribution within the body; then from eigenstrain, the residual stress is determined by means of FE. The motivation for using eigenstrain to determine residual stress in CM is that eigenstrain remains constant upon residual stress redistribution. Hence, multiple cuts can be made without changing the eigenstrain distribution [20, 23]. Implementation of the multi-axial CM involves making multiple cuts along different orientations of a continuously processed prismatic specimen. Initially, the specimen is cut into two halves as in the conventional CM. The new cut surfaces are measured, and the results are averaged. Then, the two halves are cut along their diagonal. The displacements normal to the cut surfaces are contoured and averaged. After all the measurements are completed, the eigenstrain components are obtained from these three different measured and averaged surfaces [20]. The multi-axial CM technique was successfully applied to measure residual stress in variable polarity plasma arc (VPPA)-welded plates of 2024-T35 aluminum alloy [20], thin sheets of Ti-6Al-4 V and thick laser peened plates of 316 L stainless steel [23].

The validity of CM measurements has been assessed by comparing its results with those from neutron diffraction, X-ray (lab and synchrotron) diffraction and hole drilling [15, 18, 24–26].

Recently, Pagliaro et al. [27] suggested to use superposition to determine internal residual stresses by sectioning with CM and then measuring remaining stress with other methods. This approach allows measurements in parts where the internal stress were previously difficult to access and opens up possibilities to combine the advantages of different techniques [27].

CM has found a number of applications; some of them are of particular relevance such as butt joints of S355 structural steel [28], 80-mm thick ferritic steel welds [24], 70-mm thick dissimilar metal (ferritic to austenitic) welds [15] and ferritic steel plates welded using low and very high heat input processes [25], friction stir welds between 25.4-mm thick plates of

aluminum alloys 7050-T7451 and 2024-T351 [29], 2024-T351 aluminum alloy VPPA welds [19], welded Tee-joints [22], welds of 13% Cr–4% Ni steel [30, 31], 316L stainless steel bead-on-plate specimens [32] and AA6061-T6 aluminum alloy friction stir butt welds [33].

While the sectioning technique is easier to determine residual stress over weld cross sections since almost no calculations are needed, CM provides a higher spatial resolution (1 mm spacing) [15].

CM can only be used to obtain high-resolution maps of the stress normal to the cut surface [6], but it is quite insensitive to inhomogeneities in the specimen as long as they do not significantly affect the elastic constants [29]. CM is cheap and powerful and can be used to choose appropriate measurement lines in welded structures for more detailed study, for example using neutron diffraction [7]. A further advantage of CM, compared to the few other methods that can measure a comparable stress map, is that it is relatively simple and inexpensive to perform and the equipment required is widely available [21].

2.3. Hole-drilling method

The hole-drilling method (HDM) is versatile, easy, cheap, quick and standardized [4–6, 34] and is one of the techniques most used today for measuring residual stress. The principle, proposed more than 80 years ago [35], is based on the fact that relaxation occurs if some material is removed from a part with internal residual stress and it can be evaluated through the induced local deformation. In practical terms, an hole is drilled in the component at the center of a rosette strain gauge and a suitable model is used to determine the internal stress from strain data.

HDM equipment can be laboratory-based or portable, and the technique is applicable to a wide range of materials and components.

Drill speed and feed, centering of rosette and perpendicularity to the analysis surface are the main parameters affecting the measures of internal stress; operator skill and drilling equipment also play a significant role. Today, a modern integrate measure device consists of an automatic system including an high speed turbine (up to 400,000 rpm) with tungsten carbide tools and an electric stepping motor for the vertical cutter advancement with controlled drilling speed (0.1 mm/min); a microscope endowed of two orthogonal centesimal movements for drilling the hole at the center of rosette.

The other crucial aspect is the measure of the strain through rosette strain gauges. The ASTM E837-08 standard of reference for HDM residual stress evaluation [36] prescribes three kinds of rosette (Type A, B and C) as shown in **Figure 2**.

The ASTM E837-08 standard considers both uniform and nonuniform residual stress.

The evaluation of residual stress by HDM can be done in alternative ways. Since 1988, Schajer [37] introduced the *incremental method* for evaluating the nonuniform residual stress that allows to decide the number of step and the step depth. In the cases of coating or surface

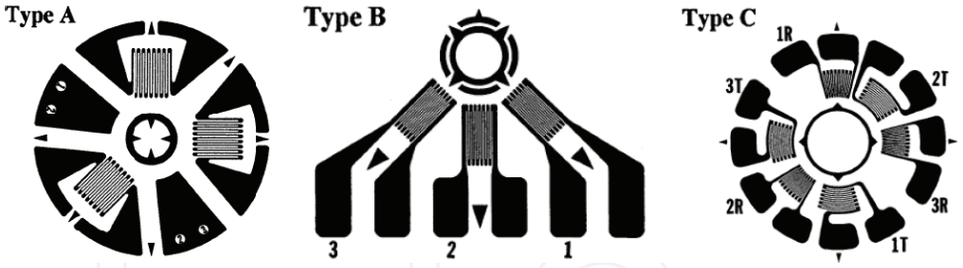

Figure 2. ASTM E837-08 standard: rosette types A, B and C.

treatment processes, for example shot peening, where more interesting is the evaluation of the residual stress in the first layer of the surface, the method permits to increase the resolution by reducing the step depth near the surface.

The *incremental deformation method*, proposed by Schwarz and Kockelmann [38], is based on the measure of the incremental deformation during drilling. In addition to the standard hole obtained by high speed milling, Kockelmann proposed also a new hole shape to be obtained by electrochemical erosion. Improvements of the mentioned methods are available in literature in terms of evaluation of relaxation strain and models. One of them, proposed by Beghini et al. [39], takes in consideration the compensation of the principal parameters affecting the accuracy in the evaluation of residual stress.

In general, for the HDM, the following experimental factors play a crucial role:

Rosette strain gauge installation: The installation needs to be performed by qualified person in compliance with the instructions of rosette and glue producer. Moreover, special attention should be paid to the cleaning of the surface where the strain gauge is bonded to avoid an alteration of the original state of residual stress.

Centering: The eccentricity between the center of the hole and the center of the rosette could introduce large error in the evaluation of residual stress.

Orthogonality and zeroing: A not accurate orthogonality between hole axis and surface could induce difference in the right measure of the depth of the hole and difficulty in zeroing.

Hole bottom fillet radius: The error in evaluating residual stress increases with the fillet radius and decreases with the depth of the hole [40].

One of the most common fields of HDM application is the evaluation of residual stress induced by welding processes. In fact, residual stress could affect the operative strength of the part, fatigue life and stress corrosion strength. In as-welded conditions, often residual stress is close to yield stress and thermal or mechanical treatments are necessary to reduce it. So, a lot of research work was done for the evaluation of residual stress in different kinds of welding processes and materials [30, 31, 40–45] with the final target to find the correct welding parameters and post processing conditions to minimize the residual stress. Some of these works use HDM as validation of nondestructive techniques such as ultrasonic [41–46], XRD [30] and neutron diffraction [31].

Pappalettere et al. [47–52] applied an electronic speckle pattern interferometry (ESPI) method to avoid the use of conventional rosette strain gauges. The ESPI is based on the correlation between two speckle patterns, each one created by the interference between a reference beam and the image of an object illuminated by a laser. Typically, the two images are of an object before and after some deformation and the technique measures the 3D displacement by evaluating the phase difference of two recorded speckle interferograms. The apparatus consists of a diode-pumped solid state laser source that generates a radiation split into two beams and focused into two monomode optical fibers. One beam is collimated through a biconvex lens and illuminates the sample, whereas the second one passes through a phase shifting piezoelectric system and then it goes to the CCD camera where interferes with the light diffused by the optically rough surface of the specimen. The camera is equipped with an optical imaging system allowing fine focusing of the image. Initial phase and final phase are evaluated by the four-step phase shifting technique. Once the initial and the final phases are determined, it is possible to calculate the amount of displacement of each point into the analysis area. **Figure 3** shows the experimental ESPI set-up [47]. In fact, rosette strain gauges introduce a not negligible cost particularly in the case where a relevant number of measurements are required. Moreover, some sources of experimental errors, such as surface preparation, bonding and positioning, are irrelevant using the not contact ESPI.

These investigators were also able to evaluate how drilling speed affects error in HDM and HDM/ESPI and concluded that higher speed helps to increase accuracy and reduce data scattering. For instance, standard deviation in residual stress evaluation in titanium samples changes from less than 3% to about 19% if drilling speed is reduced from 50,000 to 5000 rpm.

HDM was used to validate the results of the ultrasonic technique in investigations on FSW joints of 5086 plates [42], AISI 304 pipes [43] and plates [44]. The example in **Figure 4** shows the good correspondence between ultrasonic and HDM residual stress evaluation.

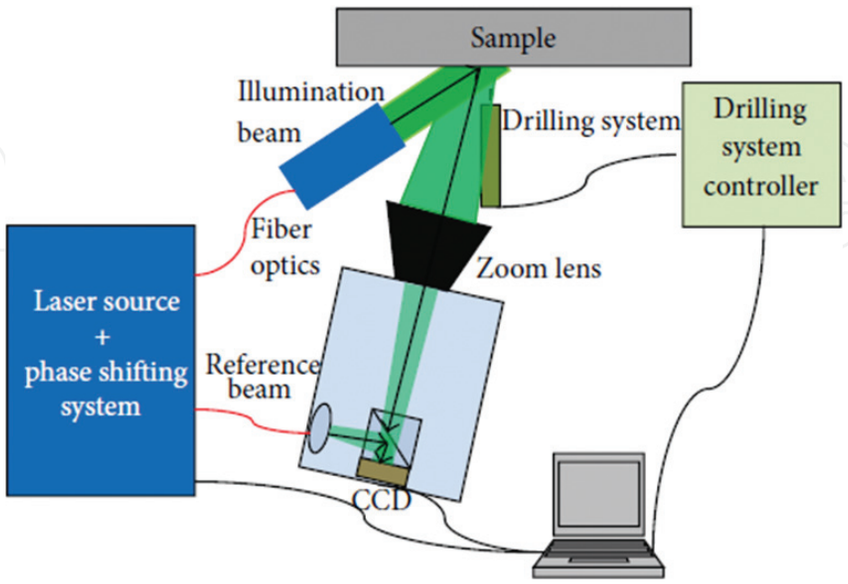

Figure 3. ESPI strain measurement set-up [47].

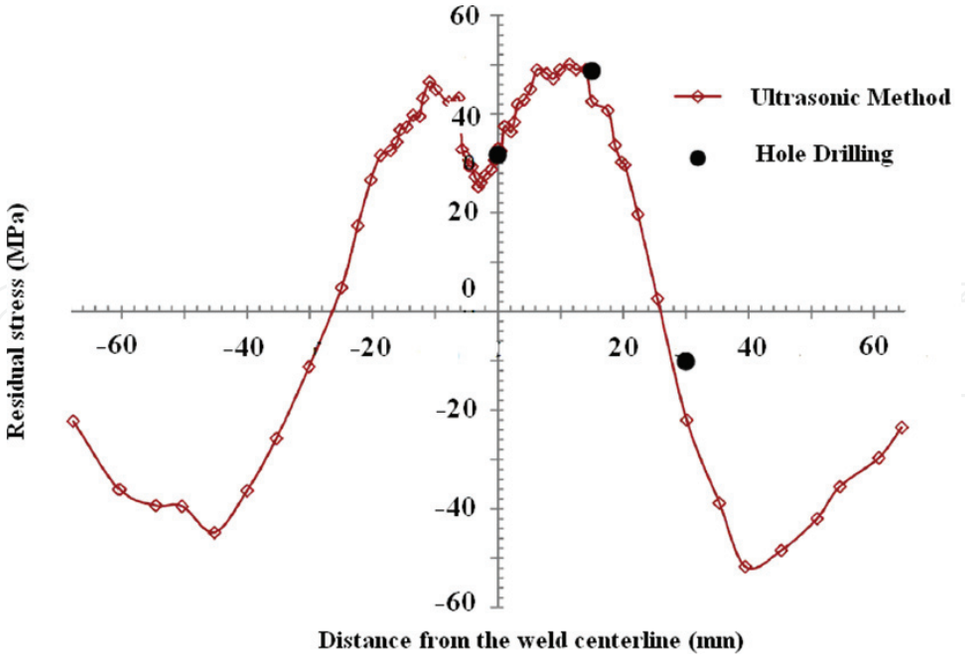

Figure 4. HDM validation of residual stress measurements performed through ultrasonic method. Redrawn from Ref. [42].

2.4. Instrumented indentation method

In the last decade, the instrumented indentation has received increasing attention for characterizing the mechanical properties of materials on a local scale. Indenters with different geometry (tetragonal Vickers pyramid, trigonal Berkovich pyramid, sphere, cone and cylinder) have been used; the following considerations refer to a sharp conical indenter (with a half apex angle α). It penetrates normally into a solid where the applied load P and penetration depth h are continuously recorded during one complete cycle of loading and unloading (**Figure 5a** and **b**).

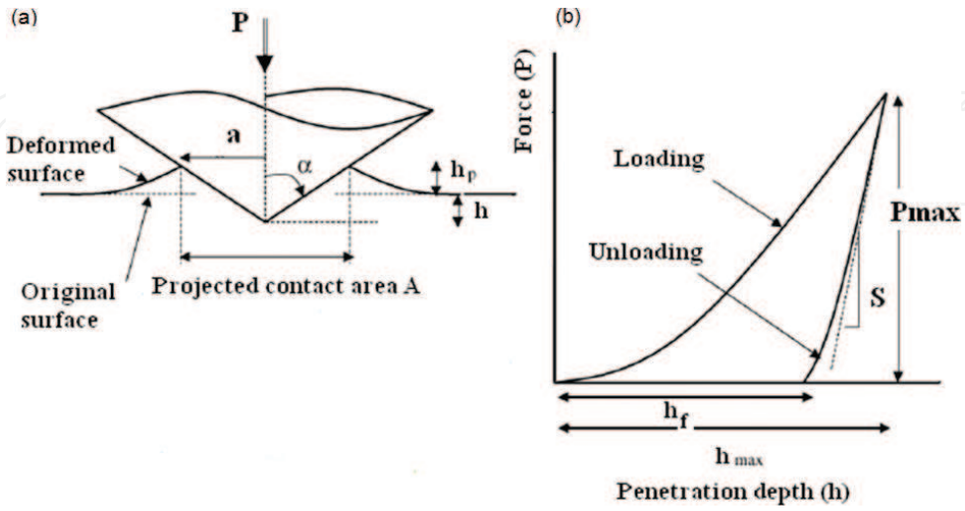

Figure 5. (a) Sketch of a sharp indentation on a homogeneous and isotropic material and (b) typical force-penetration depth curve obtained from an indentation experiment.

The contact stiffness $S = dP/dh$ is obtained from the slope of initial part of the unloading curve (**Figure 5b**).

As the indenter, a rigid cone with $\alpha = 70.3°$, penetrates the materials, either plastic pile-up at the crater rim (when the ratio between yield stress σy and Young's modulus E, $\sigma y/E$, is small) or elastic sink-in (when $\sigma y/E$ is large) is observed. The amount of pile-up/sink-in is denoted as h_p (**Figure 5a**). For conical indenters, the projected contact area A is given by:

$$A = \pi a^2 = \pi(\tan \alpha)^2 h_c^2 = 24.5 h_c^2 \tag{1}$$

where the contact depth, $h_c = h + h_p$, contains the contributions of both plastic pile-up around the indenter and elastic sink-in, which is counted negative. The pile-up and contact area can be measured experimentally or determined from numerical analysis (e.g. FE method). Once the contact area A is known, hardness H and Young's modulus E are usually obtained from the indentation curve.

Hardness H is the ratio between applied load P and contact area A *(H = P/A).*

The indentation modulus M is determined from indentation curve through the equation:

$$M = \frac{S}{2\gamma\beta\sqrt{A}}\sqrt{\pi} \tag{2}$$

where β is a shape factor ($\beta = 1$ for axisymmetric indenters and $\beta = 1.03$–1.05 for indenters with square or rectangular cross-sections) and γ is a correction factor depending on indenter geometry. In the case of the conical indenter, γ can be written as:

$$\gamma = \pi \frac{\pi/4 + 0.155 \cot\alpha \left[\frac{1-2\nu}{4(1-\nu)}\right]}{\left[\pi/2 - 0.831 \cot\alpha \left[\frac{1-2\nu}{4(1-\nu)}\right]\right]^2} \tag{3}$$

where ν is the Poisson's ratio.

For isotropic materials, the indentation modulus M corresponds to the plane-strain modulus E^*

$$M = E^* = \left(\frac{1-\nu^2}{E} + \frac{1-\nu^2{}_I}{E_I}\right) \tag{4}$$

where E_I and ν_I are the Young's modulus and Poisson's ratio of the indenter, respectively. Therefore, E can be easily calculated from M through Eq. (4).

How to correctly determine residual stresses from instrumented indentation test has been debated for some years. Initially, indentation hardness was used as a parameter of the residual stress; however, successive studies [53, 54] reported that the intrinsic hardness is invariant, regardless of the residual stress. Therefore, the change in contact morphologies with residual stress was modeled for constant maximum indentation depth assuming the independence of intrinsic hardness and residual stress [54].

The presence of residual stresses modify the indentation curve: with respect the stress-free state the same penetration depth h_t is reached at smaller load P in the case of tensile stress while compressive stress induces the opposite effect [53–55]. As shown in **Figure 6**, at the common penetration depth h_t, it is observed that P_A (with tensile stress) < P_B (stress free) < P_C (with compressive stress).

The direct comparison of the indentation curve recorded in the investigated zone with that obtained in a zone of the same material without any residual stress allows to understand the nature of the stress (tensile or compressive).

To determine the value of residual stress, we will examine in the following the case of a material with residual tensile stress; a similar analysis can be made for compressive stress.

Since the average contact pressure due to indentation, P_{ave} (equivalently, the hardness), is unaffected by any pre-existing tensile or compressive elastic stress [53], the relationship

$$P_{ave} = \frac{P}{A} = \frac{P_0}{A_0} \tag{5}$$

relates the indentation loads P and P_0 directly to the real contact areas A and A_0 of the material with and without residual stress, respectively. An equibiaxial tensile residual stress at the material surface can be considered equivalent to a tensile hydrostatic stress plus a uniaxial compressive stress component, $-\sigma_H$ (see **Figure 6**). This compressive stress component induces a differential indentation force $\sigma_H A$ acting in the same direction as the indentation load P. On these grounds, a tensile residual stress aids indentation by lowering the indentation load needed to penetrate the material to a given depth, as compared to the virgin material.

From the initial part of the unloading curve, the real contact area A at maximum load P_{max} for the material with the residual stress is

$$A = \left(\frac{dP}{dh}\frac{1}{cE^*}\right)^2 \tag{6}$$

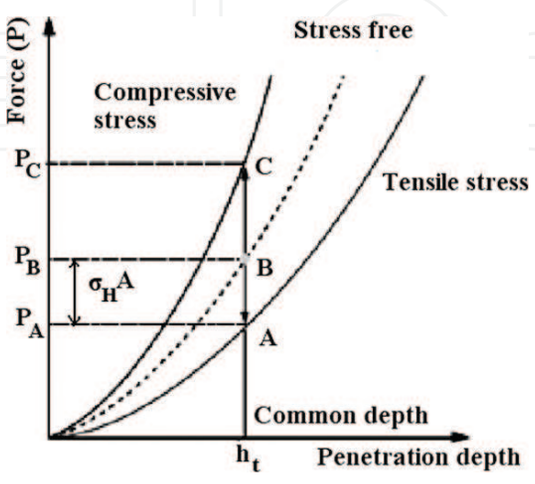

Figure 6. Effect of stress states on the indentation loading curve.

where c is a constant depending on the indenter geometry (c = 1.167 for Berkovich indenter, c = 1.142 for the Vickers indenter). An analogous relationship is found for the unstressed material; thus, it can be easily demonstrated that

$$\frac{A}{A_0} = \left(\frac{dP}{dh}\right)^2 \left(\frac{dP_0}{dh_0}\right)^{-2} = \left(1 + \frac{\sigma_H}{P_{ave}}\right)^{-1} \tag{7}$$

where P_{ave} is the average pressure.

The ratio A/A_0 is determined from the initial slopes of the unloading parts of the P-h curves. The value of A is calculated through Eq. (6), and at $P = P_{\max}$, the average pressure $P_{ave} = P_{max}/A$. The residual stress magnitude σ_H is found by introducing the calculated values of A/A_0 and P_{ave} into Eq. (7).

The stress determined in this way is that of a layer of depth h_{max} corresponding to P_{max} and represents an average value over the layer. With the availability of macro-, micro- and nanoindenters, instrumented indentation can be used to probe local properties at different size scales.

The technique has been successfully used for determining residual stresses in different metallic alloys and recently also in tissues and other soft biological materials (e.g. see [56]).

Owing to its specific characteristics, indentation is quite useful for investigating welded mechanical parts because it allows to determine the residual stress on local scale, namely in the melted and heat affected zones of the joints. Instrumented indentation was applied by Jang et al. [57] for evaluating residual stress in A335 P12 steel welds in electric power plant facilities before and after stress-relaxation annealing. Comparison with the results of conventional saw-cutting tests showed the efficiency of indentation tests. The method was employed by Ullner et al. [58] to determine the local stresses in resistance-spot welded joints of advanced high strength steels.

3. Nondestructive techniques

3.1. Barkhausen noise method

Magnetic methods rely on the interaction between magnetization and elastic strain in ferromagnetic materials; they are sensitive to all three types of residual stress, but cannot distinguish between them. Here, only the Barkhausen noise (BN) method, based on the analysis of magnetic domain wall motion, will be presented and discussed.

Ferromagnetic materials consist of magnetically ordered regions called domains; each domain is magnetized along a certain direction and is separated from the others by walls where the direction of magnetization abruptly turns. The net magnetization of a material is the average of the magnetizations within all domains.

Under the action of an external magnetic field, the domain walls move and the resulting change in magnetization is detected as electrical pulses in a coil placed near the material

surface. The process is not continuous but consists of small steps generated by domains jumping from one position to another. Pulses are random in amplitude, duration and temporal separation and give rise to a noise-like signal called Barkhausen noise.

BN is exponentially damped as a function of the traveled distance inside the material and the extent of damping determines the depth from which information can be obtained. Such depth mainly depends on the signal frequency together with conductivity and magnetic permeability of the tested material. Measurement depths in steels range from 0.01 to 3.0 mm; since this value is much higher than that of X-ray diffraction (some tens of microns), the BN method allows to quantify subsurface stress without need of removing the surface layer.

The intensity of BN depends on both stress and microstructure of the material; thus, a suitable calibration is of the utmost importance to properly determine uniaxial and biaxial surface stresses. Grain size, texture and dislocation structures play an important role in BN response; therefore, it is necessary to separate the contribution of stress from that of microstructure through a suitable calibration procedure. Calibration involves measurement of the BN signal on a representative section of the sample material using a known applied stress. A typical uniaxial calibration curve, taken from Kesavan et al. [9], is shown in **Figure 7**. The handbook [3] reports more details of uniaxial and biaxial stress calibration procedures and related results for isotropic and anisotropic materials.

As a result of magnetoelastic interaction, in materials with positive magnetic anisotropy (most steels and cobalt alloys), compressive stresses decrease the BN intensity, whereas tensile stresses increase it. Therefore, the measurement of BN intensity allows to determine the amount of residual stress and also defines the direction of principal stresses.

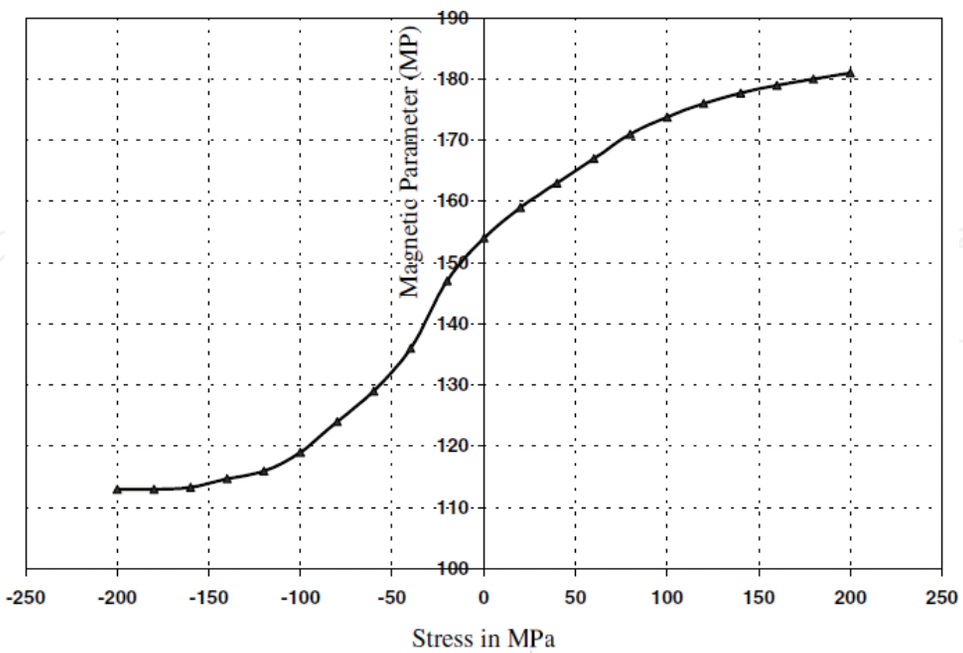

Figure 7. Typical uniaxial calibration curve taken from Ref. [9].

The advantages of the BN method for stress measurements in welds are that it is fast, reliable and requires no specific surface preparation. Moreover, it can be used for continuous monitoring of stress in industrial processes. A significant example is reported in **Figure 8** showing the effect of furnace stress relieving on a welded "T" section [3]; it is noteworthy that the stress profiles of the two seams before stress relieving are asymmetric because the left seam was welded first, being then subjected to a strong heating during the realization of the right seam.

Vourna et al. [59–61] examined through the BN method joints of an electrical steel (Si 2.18 wt%) welded by means of three different techniques, namely Tungsten Inert Gas (TIG), Plasma and Electron Beam, determining maps of residual stress across melted zone, heat affected zone and base material. The comparison of results with those from X-ray diffraction showed a good agreement. Similar good results were achieved by measurements performed on other types of steels such as API X65 [62], API 5 L X70 [63], AS1548–7-460R [64], structural steel [65] and Cr-Mo steel [66]. As pointed out by many investigators who examined welds of different steels, BN technique requires a precise calibration procedure in all zones, which have a noticeably different microstructure, namely each zone should be separately considered for calibration [59, 60, 61, 63].

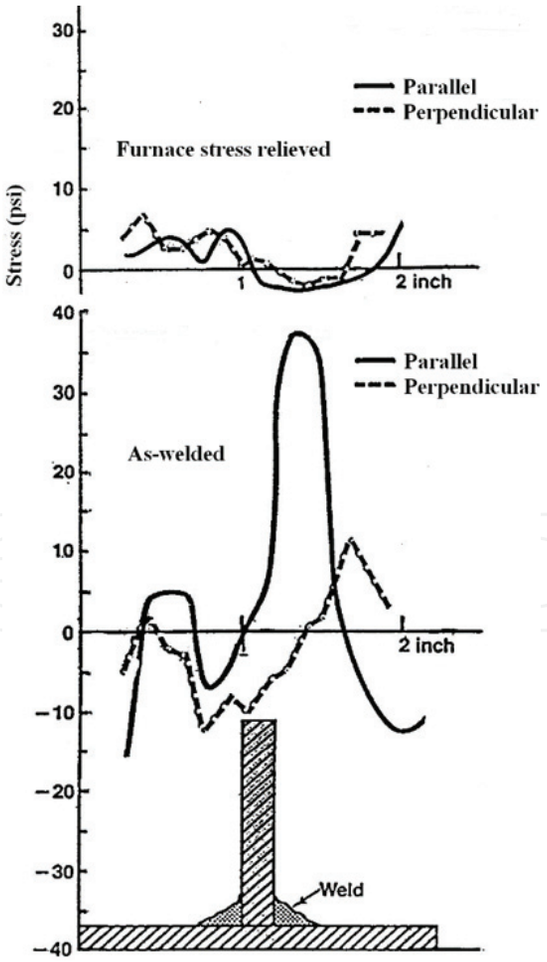

Figure 8. Stress relieving on a welded "T" section measured through BN; redrawn from Ref. [3].

The potential of BN technique for directly assessing fatigue processes and progressive residual stress relaxation in cyclically loaded welds has been shown by Lachmann et al. [67].

Beside the aforesaid advantages of the BN technique, some drawbacks place a severe restriction on its general applicability: (i) the material must be ferromagnetic; (ii) the total range of stress sensitivity (~ 6 MPa) is low; (iii) the measurement depth is limited to the surface layers and (iv) BN signal saturation may occur when tests are carried out on martensitic steels with very fine and complex microstructural features.

3.2. Ultrasonic method

The ultrasonic techniques are based on variations in the velocity of ultrasonic waves, which can be related to the residual stress state through the elastic constants of the material [34, 44]. Like the magnetic methods, the ultrasonic techniques are sensitive to all three kinds of residual stress, but are not able to distinguish between them.

Ultrasonic stress measurement is founded on the linear relation between velocity of the ultrasonic wave and the material stress. This correlation, known as the acoustoelastic effect, establishes the following relationship between the velocity V and the stress σ:

$$V = V_0 + K\sigma \tag{8}$$

where K is the acoustoelastic constant (AEC) depending on the material and V_0 and V are the velocities in stress-free and stressed material, respectively [3].

In 1967, Crecraft showed that the acoustoelastic law can be employed for stress measurement of engineering materials [35, 42, 45]. Changes in ultrasonic speed can be observed when a material is subjected to a stress, the changes providing a measure of the stress averaged along the wave path. The acoustoelastic coefficients necessary for the analysis are usually calculated using calibration tests. Different types of wave can be employed but the commonly used technique is the longitudinal critically refracted (Lcr) wave method [4]. The Lcr wave is an acoustical wave that is excited when the angle of incidence is slightly smaller than the first critical angle, which is calculated from the Snell's law [44, 68, 69]. It is a bulk longitudinal wave, traveling just below the surface of the specimen. This wave is more sensitive to stress and less sensitive to localized material texture changes [69]. Different ultrasonic configurations can be employed for residual stresses measurements by Lcr technique. As a common experimental setup, longitudinal waves are propagated at the first critical angle by a transmitter transducer and then travel parallel the tested material surface and finally are detected by a receiver transducer. The residual stress in a subsurface layer is measurable while the depth of layer is related to the ultrasonic wavelength, often exceeding a few millimeters [43]. The relation between measured travel-time change of Lcr wave and the corresponding uniaxial stress was derived by Egle and Bray [70]; with knowledge of the weld induced change in travel time and the measured acoustoelastic constant, the stress produced by the weld may be calculated [43]. The principal steps to be followed in the measurement of residual stress by ultrasonic methods are: (i) selection of weld joint or component; (ii) determination of the acoustoelastic constant (AEC) of the material using standard tensile specimen by applying

varying loads; (iii) ultrasonic velocity measurements in the weld joint or component of interest and (iv) determination of residual stress using AEC [68].

Javadi et al. [41–43] carried out a series of interesting studies on the ultrasonic method. They compared contact and immersion ultrasonic measurements of welding residual stress in dissimilar joints. A combination of FE welding simulation and Lcr ultrasonic waves was employed to reach the goal, and on the basis of experimental results, they concluded that both of the methods can measure the residual stress with an acceptable accuracy and the selection between them depends on geometry and dimensions of tested structure and also on the available experimental devices [41].

The same investigators developed a method (TLcr) that is the combination of Taguchi method (a technique to optimize welding parameters) and the Lcr ultrasonic method in order to study which process parameter has the highest effect on the longitudinal residual stresses in aluminum plates joined by the FSW process [42]. Finally, Javadi et al. [43] studied the combination of FE and Lcr method (known as FELCR) confirming its ability to evaluate the pipe residual stresses through the thickness.

The ultrasonic technique was also successfully used in the study of residual stress in dissimilar joints [41]; residual stress through the thickness of stainless steel plates with 10 mm thickness [44]; longitudinal residual stress through the thickness of aluminum plates with 8 mm thickness [45]; for assessment of surface/subsurface longitudinal residual stresses in AISI type 316LN stainless steel weld joints made by ATIG and TIG welding processes [68]; welding residual stress through the thickness of stainless steel pipe [43] and prediction of total residual stress and fusion boundary in three pass welded stainless steel plates [71].

In conclusion, the ultrasonic technique is nondestructive, sensitive to microstructures and defects, has sufficiently good spatial resolution (5 mm) for longitudinal residual stresses across welded joints and is easy and simple to use and cost effective [8, 69, 72]. Additionally, the instrumentation is portable and quick to implement [34] and it is well suited for routine inspection procedures and industrial studies of large components, such as steam turbine discs [4]. On the other hand, this method has some difficulties in separating the effects of multiaxial stresses and in measuring the stress in an exact depth; since the penetration depths of the ultrasonic transducers are limited to a few millimeters, measurement of thick materials on both sides is recommended.

3.3. X-ray and neutron diffraction method

X-ray and neutron diffraction methods are based on the measurement of lattice strains by studying the variations of lattice spacings of the polycrystalline material. In other words, these techniques allow to determine the variations of lattice spacings induced by compressive or tensile stresses and to calculate the stresses from the strains, known the elastic constants of the material under investigation. Neutron and X-ray wavelengths used in diffraction experiments are about of the same magnitude; however, neutron diffraction differs from X-ray diffraction in several ways. Two aspects are of particular relevance to the present discussion:

1. The penetration depth in a material of a neutron beam is of the order of some centimeters and that of X-rays is of tens of microns. Therefore, X-ray diffraction measures the residual strain on the surface of the material, whereas neutron diffraction measures the residual strain within a volume of the sample. Owing to its unique deep penetration, neutron diffraction has been used to measure stresses in welds of 50-mm thick steel plates [73]. High energy X-rays from synchrotron sources have the penetration depth in between and are used to investigate subsurface stresses.
2. The intensities of X-ray diffraction lines depend on the atomic scattering factor *f*, which is directly proportional to the atomic number Z; thus, in a polyphasic material, the phases rich of light elements will exhibit diffraction patterns of lower intensity with respect to those rich of heavy elements. For instance, in a steel with perlitic structure (ferrite plus cementite), only the diffraction lines of ferrite are revealed, whereas those of cementite have a negligible intensity, comparable with background.

In the case of neutrons, scattering intensity varies quite irregularly with the atomic number Z; therefore, elements with quite different values of Z may scatter neutrons equally well. Furthermore, some light elements, such as carbon, scatter neutrons more intensely than some heavy elements. It follows that structure analyses can be carried out with neutron diffraction that are impossible, or possible only with great difficulty, with X-ray.

Both neutron and X-ray diffraction techniques can be used to study all three kinds of stresses. The peak shift method is sensitive to σ^{I}, whereas line broadening is sensitive to σ^{II} and σ^{III}.

Residual stresses in polycrystalline materials change the lattice spacings, which vary according to the orientation of planes relatively to the stress direction. In fact, the crystal lattice is used as a strain gauge. The elastic strain can be calculated from the variation of lattice spacing d: d_0, determined by the position of the Bragg peak of stressed (θ) and stress-free (θ_0) material:

$$\varepsilon = \frac{d - d_0}{d_0} = -\Delta\theta \cot\theta \tag{9}$$

The strain measured from shift of peak position is the elastic strain along the normal direction to diffracting planes, i.e. those parallel to the surface of the examined sample.

The $\sin^2\psi$ method allows to determine the stress along any direction Φ in the plane XY (**Figure 9**).

The direction Φ is the projection on the plane XY of the direction OO′ forming an angle ψ with the axis Z. The stress σ_Φ is given by:

$$\sigma_\varphi = \frac{d_\psi - d_z}{d_z} \cdot \frac{E}{(1+\nu)\sin^2\psi} \tag{10}$$

and is determined by measuring d_ψ and d_z, known E and ν. Through X-ray and neutron diffraction, it is possible to measure uniaxial, biaxial and triaxial stress states, an exhaustive treatment of the topic can be found in Ref. [3].

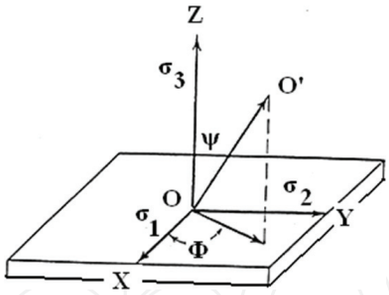

Figure 9. The direction Φ is the projection on the plane XY of the direction forming an angle ψ with the axis Z.

Since the Warren Averbach method [74] appeared in the 1950s, diffraction line broadening analysis is used to study the microstructural evolution of crystalline materials. Two factors contribute to line broadening: (i) the size of coherently diffracting domains (grains, sub-grains or cells) and (ii) micro-strains related to the density of dislocations, stacking faults and twins. Of course, line broadening is related to σ^{II} and σ^{III} and a lot of specific literature does exist on the matter; thus, we will not treat here the details of analysis.

X-ray and neutron diffraction has been extensively used to investigate stress state in welds realized with different techniques and materials (steels [73, 75–81], aluminum alloys [82–87], titanium alloys [88, 89] and other alloys). Remarkable results have been achieved; for instance, neutron and synchrotron X-ray diffraction has been successfully used for mapping residual stresses in welded parts (e.g. see [90]).

Woo et al. [86] were able to determine the evolution of temperature and thermal stresses during friction stir welding of Al6061-T6 through in situ, time-resolved neutron diffraction technique. The method allows to deconvolute the temperature and stress from the lattice spacing changes measured by neutron diffraction.

Two case studies taken from the research activity of the authors are now presented to illustrate the application of the technique.

3.3.1. Case study 1

Electron beam (EB) welding has been used to realize seams on 2-mm thick plates of directionally solidified IN792 superalloy [91–93]. The experiments evidenced the importance of pre-heating the workpieces to avoid the formation of long cracks in the seam and X-ray diffraction (XRD) was used to identify the better pre-heating temperature (PHT). The samples were mounted on a micrometric translating table that allowed to move the samples and irradiate the desired zone.

XRD spectra were collected by focusing the beam on melted zone and **Figure 10** compares the {220} peak profiles of samples welded with PHT of 200 and 300°C at the same pass speed (1.5 m/min).

The vertical line indicates the peak position of stress-free base material. The peak position of the sample welded with PHT = 300°C almost corresponds to that of stress-free material (vertical line), whereas the peak position of sample welded with PHT = 200°C is shifted to lower angles

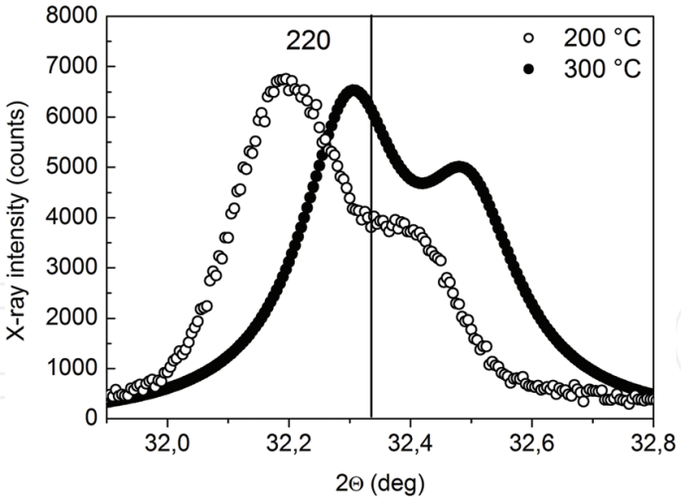

Figure 10. {220} peak profiles collected from melted zone of samples welded at the same pass speed of 1.5 m/min with PHT of 200 and 300°C. The vertical line indicates the peak position of base material free from the stresses arising from welding [93].

indicating the presence of tensile stresses. On the basis of these results, the pre-heating of the plates at 300°C was identified as the optimal condition to realize EB joints of IN792 DS superalloy.

3.3.2. Case study 2

Case study 2 presents a study on a joint with a very complex structure. Because of its high melting point and good thermal conductivity, W is a promising armor material for protecting the components of International Thermonuclear Experimental Reactor (ITER) from plasma damage. However, the joining of W to other metals is challenging for the lower thermal expansion of W, its high elastic modulus and brittleness. An experimental campaign has been carried out by authors for realizing thick W-coatings on different metals, and Plasma Spraying was used as deposition technique for its simplicity, the possibility to cover complex and extended surfaces and the relatively low cost. The reported example regards 5-mm thick W coatings deposited on CuCrZr alloy. An appropriate interlayer was optimized to increase the adhesion of W on the metallic substrate and to provide a soft interface with intermediate thermal expansion coefficient for better thermo-mechanical compatibility. The bonding interface with thickness of ~800 μm was realized through successive deposition steps. It consists of a layer of pure Ni (thickness ~200 μm) directly on the CuCrZr substrate followed by a stratification of thinner layers (thickness ~30 μm) obtained by spraying grading mixtures of Al–12% Si, Ni–20% Al, Ni–20% Al and W powders. A detailed description is given in [94, 95].

To verify the quality of joints, high temperature X-ray diffraction (HT-XRD) has been employed at increasing temperatures up to 425°C and XRD spectra are shown in **Figure 11**. The vertical lines indicate the peak positions of the strain-free metals at room temperature.

The positions of Cu and W peaks at 25°C correspond to those of the stress-free condition, whereas Al and Ni peaks exhibit significant shifts. This means that residual strains are present in the interlayer but not in coating and substrate. At 425°C, all the peaks move towards lower

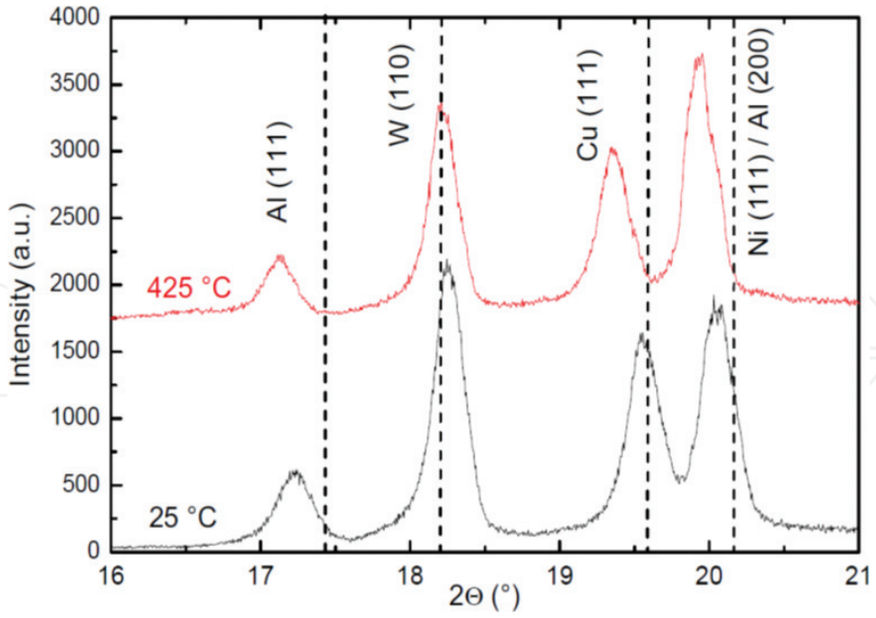

Figure 11. XRD spectra collected from W-CuCrZr system. The markers indicate the peak positions of stress-free metals (JCPDS-ICDD database).

angles, in part due to thermal expansion. **Table 1** shows the strains, corrected from the effect of thermal expansion, which are quite different in the metals of the system W-CuCrZr. Among them, W exhibits the lowest strain level (~ 5×10^{-4}) both at 25 and 425°C; thus, strain substantially does not change as temperature increases. At room temperature, also the strain of Cu is low (~ 1×10^{-3}) but it increases at 425°C. In the interlayer, a different behavior between Ni and Al is observed: the strain level in Al is about one order of magnitude higher than that of Ni.

Such results are very interesting if one considers that cracks form in W near the interlayer and then propagate by a brittle and transgranular fracture mechanism towards the substrate. In fact, they demonstrate that interlayer properly works by accumulating stress and protecting the coating. On this basis, HT-XRD permits to evaluate the quality of the deposition and can be used to orientate the work for optimizing structure and composition of the interlayer and to find the right parameters of deposition process.

Metal.	**$\varepsilon \times 10^3$**	
T (°C)	**25°C**	**425°C**
Al	13.30	10.20
W	0.51	0.54
Cu	0.94	4.42
Ni	1.25	1.92

Table 1. Strains at 25 and 425°C.

Author details

Roberto Montanari[1]*, Alessandra Fava[1] and Giuseppe Barbieri[2]

*Address all correspondence to: roberto.montanari@uniroma2.it

1 Department of Industrial Engineering, University of Rome Tor Vergata, Rome, Italy

2 Department of Sustainability, ENEA Centro Ricerche Casaccia, Santa Maria di Galeria, Italy

References

[1] Coyle RA. The measurement of residual stress. Non-Destructive Testing. 1984;**21**:6-9

[2] Finch DN. A Review of Non-destructive Residual Stress Measurement Techniques. Leatherhead, Surrey, UK: ERA Technology Ltd; 1994

[3] Lu J. Handbook of Measurement of Residual Stresses. USA: Society for Experimental Mechanics. The Fairmont Press Inc.; 1996. ISBN: 0-88173-229-X

[4] Withers PJ, Bhadeshia HKDH. Residual stress Part 1 – Measurement techniques. Materials Science and Technology. 2001;**17**:355-365. DOI: 10.1179/026708301101509980

[5] Withers PJ, Bhadeshia HKDH. Residual stress Part 2 – Nature and origins. Materials Science and Technology. 2001;**17**:366-375. DOI: 10.1179/026708301101510087

[6] Rossini NS, Dassisti M, Benyounis KY, Olabi AG. Methods of measuring residual stresses in components. Materials & Design. 2012;**35**:572-588. DOI: 10.1016/j.matdes.2011.08.022

[7] Withers PJ, Turski M, Edwards L, Bouchard PJ, Buttle DJ. Recent advances in residual stress measurement. International Journal of Pressure Vessels and Piping. 2008;**85**:118-127. DOI: 10.1016/j.ijpvp.2007.10.007

[8] Huang X, Liu Z, Xie H. Recent progress in residual stress measurement techniques. Acta Mechanica Solida Sinica. 2013;**26**:570-583. DOI: 10.1016/S0894-9166(14)60002-1

[9] Kesavan K, Ravisankar K, Parivallal S, Sreeshylam P. Non destructive evaluation of residual stresses in welded plates using the Barkhausen noise technique. Experimental Techniques. 2005;**29**:17-21. DOI: 10.1111/j.1747-1567.2005.tb00234.x

[10] Tebedge N, Alpsten G, Tall L. Residual-stress measurement by the sectioning method – A procedure for residual-stress measurements by the sectioning method is described. Two different hole-drilling methods were performed and the results are compared. Experimental Mechanics. 1973;**13**:88-96. DOI: 10.1007/BF02322389

[11] Alpsten GA, Tall L. Residual stresses in heavy welded shapes. Welding Research Supplement. 1970;**49**:93s-105s

[12] Wang Y-B, Li G-Q, Chen S-W. The assessment of residual stresses in welded high strength steel box sections. Journal of Constructional Steel Research. 2012;**76**:93-99. DOI: 10.1016/j.jcsr.2012.03.025

[13] Tsai CL, Park SC, Cheng WT. Welding distortion of a thin-plate panel structure. Welding Journal. 1999;**78**:156s-165s

[14] Prime MB. Cross-sectional mapping of residual stresses by measuring the surface contour after a cut. Journal of Engineering Materials and Technology. 2000;**123**:162-168. DOI: 10.1115/1.1345526

[15] Woo W, An GB, Truman CE, Jiang W, Hill MR. Two-dimensional mapping of residual stresses in a thick dissimilar weld using contour method, deep hole drilling, and neutron diffraction. Journal of Materials Science. 2016;**51**:10620-10631. DOI: 10.1007/s10853-016-0283-z

[16] Prime MB, Hill MR, DeWald AT, Sebring RJ, Dave VR, Cola MJ. Residual stress mapping in welds using the contour method. In: Proceedings of the 6th International Conference; 15–19 April 2002; Pine Mountain, Georgia: ASM International; 2003. p. 891-896

[17] Shin SH. FEM analysis of plasticity-induced error on measurement of welding residual stress by the contour method. Journal of Mechanical Science and Technology. 2005;**19**:1885-1890. DOI: 10.1007/BF02984267

[18] Brown DW, Holden TM, Clausen B, Prime MB, Sisneros TA, Swenson H, Vaja J. Critical comparison of two independent measurements of residual stress in an electron-beam welded uranium cylinder: Neutron diffraction and the contour method. Acta Materialia. 2011;**59**:864-873. DOI: 10.1016/j.actamat.2010.09.022

[19] Zhang Y, Ganguly S, Edwards L, Fitzpatrick ME. Cross-sectional mapping of residual stresses in a VPPA weld using the contour method. Acta Materialia. 2004;**52**:5225-5232. DOI: 10.1016/j.actamat.2004.07.045

[20] Kartal ME, Liljedahl CDM, Gungor S, Edwards L, Fitzpatrick ME. Determination of the profile of the complete residual stress tensor in a VPPA weld using the multi-axial contour method. 2008;**56**:4417-4428. DOI: 10.1016/j.actamat.2008.05.007

[21] Prime MB, Sebring RJ, Edwards JM, Hughes DJ, Webster PJ. Laser surface-contouring and spline data-smoothing for residual stress measurement. Experimental Mechanics. 2004;**44**:176-184. DOI: 10.1177/00144851039762

[22] Murugan N, Narayanan R. Finite element simulation of residual stresses and their measurement by contour method. Materials and Design. 2009;**30**:2067-2071. DOI: 10.1016/j.matdes.2008.08.041

[23] DeWald AT, Hill MR. Multi-axial contour method for mapping residual stresses in continuously processed bodies. Experimental Mechanics. 2006;**46**:473-490. DOI: 10.1007/s11340-006-8446-5

[24] Woo W, An GB, Em VT, De Wald AT, Hill MR. Through-thickness distributions of residual stresses in an 80 mm thick weld using neutron diffraction and contour method. Journal of Materials Science 2015;**50**:784-793. DOI: 10.1007/s10853-014-8638-9

[25] Woo W, An GB, Kingston EJ, DeWald AT, Smith DJ, Hill MR. Through-thickness distributions of residual stresses in two extreme heat-input thick welds: A neutron diffraction, contour method and deep hole drilling study. Acta Materialia. 2013;**61**:3564-3574. DOI: 10.1016/j.actamat.2013.02.034

[26] Woo W, Feng Z, Wang XL, David SA. Neutron diffraction measurements of residual stresses in friction stir welding: A review. Science and Technology of Welding & Joining. 2011;**16**:23-32. DOI: 10.1179/136217110X12731414739916

[27] Pagliaro P, Prime MB, Robinson JS, Clausen B, Swenson H, Steinzig M, Zuccarello B. Measuring inaccessible residual stresses using multiple methods and superposition. Experimental Mechanics. 2011;**51**:1123-1134. DOI: 10.1007/s11340-010-9424-5

[28] Braga DFO, Coules HE, Pirling T, Richter-Trummer V, Colegrove P, de Castro PMST. Assessment of residual stress of welded structural steel plates with or without post weld rolling using the contour method and neutron diffraction. Journal of Materials Processing Technology. 2013;**213**:2323-2328. DOI: 10.1016/j.jmatprotec.2013.07.004

[29] Prime MB, Gnäupel-Herold T, Baumann JA, Lederich RJ, Bowden DM, Sebring RJ. Residual stress measurements in a thick, dissimilar aluminum alloy friction stir weld. Acta Materialia. 2006;**54**:4013-4021. DOI: 10.1016/j.actamat.2006.04.034

[30] Thibault D, Bocher P, Thomas M. Residual stress and microstructure in welds of 13% Cr–4% Ni martensitic stainless steel. Journal of Materials Processing Technology. 2009;**209**: 2195-2202. DOI: 10.1016/j.jmatprotec.2008.05.005

[31] Thibault D, Bocher P, Thomas M, Gharghouri M, Côté M. Residual stress characterization in low transformation temperature 13% Cr–4% Ni stainless steel weld by neutron diffraction and the contour method. Materials Science and Engineering A. 2010;**527**:6205-6210. DOI: 10.1016/j.msea.2010.06.035

[32] Turski M, Edwards L. Residual stress measurement of a 316l stainless steel bead-on-plate specimen utilising the contour method. International Journal of Pressure Vessels and Piping. 2009;**86**:126-131. DOI: 10.1016/j.ijpvp.2008.11.020

[33] Liu C, Yi X. Residual stress measurement on AA6061-T6 aluminum alloy friction stir butt welds using contour method. Materials and Design. 2013;**46**:366-371. DOI: 10.1016/j.matdes.2012.10.030

[34] Kandil FA, Lord JD, Fry AT, Grant PV. Review of Residual Stress Measurement Methods – A Guide to Technique Selection. NPL Report MATC(A)04. National Physical Laboratory, Teddington, Middlesex, UK; 2001

[35] Ruud CO. A review of selected non-destructive methods for residual stress measurement. NDT International. 1982;**15**:15-23. DOI: 10.1016/0308-9126(82)90083-9

[36] ASTM E837-08. Standard Test Method for Determining Residual Stresses by the Hole-Drilling Strain Gage Method. West Conshohocken, PA: ASTM International; 2009. DOI: 10.1520/E0837-08E02

[37] Schajer GS. Application of finite element calculations to residual stress measurements. Journal of Engineering Materials and Technology. 1981;**103**:157-163. DOI: 10.1115/1.3224988

[38] Schwarz T, Kockelmann H. The hole drilling method – The best technique for the experimental determination of residual stresses in many fields of application. Messtechnische Briefe. 1993;**29**:33-38

[39] Beghini M, Bertini L, Mori LF. Evaluating non-uniform residual stress by the hole-drilling method with concentric and eccentric holes. Part II: Application of the influence functions to the inverse problem. Strain. 2010;**46**:337-346. DOI: 10.1111/j.1475-1305.2009.00684.x

[40] Scafidi M, Valentini E, Zuccarello B. Effect of the hole-bottom fillet radius on the residual stress analysis by the hole drilling method. ICRS-8 – The 8th International Conference on Residual Stress; 6-8 August 2008; Denver, CO (USA). Newtown Square: JCPDS – International Centre for Diffraction Data; 2009. p. 263-270

[41] Javadi Y, Najafabadi MA. Comparison between contact and immersion ultrasonic method to evaluate welding residual stresses of dissimilar joints. Materials and Design. 2013;**47**:473-482. DOI: 10.1016/j.matdes.2012.12.069

[42] Javadi Y, Sadeghi S, Najafabadi MA. Taguchi optimization and ultrasonic measurement of residual stresses in the friction stir welding. Materials and Design. 2014;**55**:27-34. DOI: 10.1016/j.matdes.2013.10.021

[43] Javadi Y, Pirzaman HS, Raeisi MH, Najafabadi MA. Ultrasonic inspection of a welded stainless steel pipe to evaluate residual stresses through thickness. Materials and Design. 2013;**49**:591-601. DOI: 10.1016/j.matdes.2013.02.050

[44] Javadi Y, Akhlaghi M, Najafabadi MA. Using finite element and ultrasonic method to evaluate welding longitudinal residual stress through the thickness in austenitic stainless steel plates. Materials and Design. 2013;**45**:628-642. DOI: 10.1016/j.matdes.2012.09.038

[45] Sadeghi S, Najafabadi MA, Javadi Y, Mohammadisefat M. Using ultrasonic waves and finite element method to evaluate through-thickness residual stresses distribution in the friction stir welding of aluminum plates. Materials and Design. 2013;**52**:870-880. DOI: 10.1016/j.matdes.2013.06.032

[46] Ya M, Marquette P, Belahcene F, Lu J. Residual stresses in laser welded aluminium plate by use of ultrasonic and optical methods. Materials Science and Engineering A. 2004;**382**:257-264. DOI: 10.1016/j.msea.2004.05.020

[47] Barile C, Casavola C, Pappalettera G, Pappalettere C. Analysis of the effects of process parameters in residual stress measurements on titanium plates by HDM/ESPI. Measurement. 2014;**48**:220-227. DOI: 10.1016/j.measurement.2013.11.014

[48] Casavola C, Pappalettere C, Tursi F. Analytical study of strain's random error on residual stresses calculated by hole drilling method. 10th Youth Symposium on Experimental Solid Mechanics; 25–28 May 2011; Chemnitz, Germany. New York: Curran Associates, Inc.; 2014. p. 111-113

[49] Barile C, Casavola C, Pappalettera G, Pappalettere C. Consideration on temperature fields and internal radius of analysis in hdm+espi residual stress measurements. XIIIth Youth Symposiumon Experimental Solid Mechanics; 29 June–02 July 2014; Děčin, Czech Republic. New York: Curran Associates, Inc.; 2015. p. 11-14

[50] Barile C, Casavola C, Pappalettera G, Pappalettere C. Considerations on the choice of experimental parameters in residual stress measurements by hole-drilling and ESPI. Frattura ed Integrità Strutturale. 2014;**30**:211-219. DOI: 10.3221/IGF-ESIS.30.27

[51] Casavola C, Campanelli SL, Pappalettere C. Experimental analysis of residual stresses in the selective laser melting process. In: Proceedings of the XIth International Congress and Exposition; 2–5 June 2008; Orlando, Florida, USA: Society for Experimental Mechanics Inc.; 2008

[52] Barile C, Casavola C, Pappalettera G, Pappalettere C. Remarks on residual stress measurement by hole-drilling and electronic speckle pattern interferometry. The Scientific World Journal. 2014;**2014**:1-7. DOI: 10.1155/2014/487149

[53] Suresh S, Giannakopoulos AE. New method for estimating residual stresses by instrumented sharp indentation. Acta Materialia. 1998;**46**:5755-5767. DOI: 10.1016/S1359-6454(98)00226-2

[54] Tsui TY, Oliver WC, Pharr GM. Influences of stress on the measurement of mechanical properties using nanoindentation: Part I. Experimental studies in an aluminum alloy. Journal of Materials Research. 1996;**11**:752-759. DOI: https://doi.org/10.1557/JMR.1996.0091

[55] Lee Y-H, Kwon D. Residual stresses in DLC/Si and au/Si systems: Application of a stress-relaxation model to the nanoindentation technique. Journal of Materials Research. 2002; **17**:901-906. DOI: https://doi.org/10.1557/JMR.2002.0131

[56] Boccaccio A, Papi M, De Spirito M, Lamberti L, Pappalettere C. Effect of the residual stress on soft sample nanoindentation. Applied Physics Letters 2013;**102**. DOI: 10.1063/1.4801428

[57] J-I J, Son D, Lee Y-H, Choi Y, Kwon D. Assessing welding residual stress in A335 P12 steel welds before and after stress-relaxation annealing through instrumented indentation technique. Scripta Materialia. 2003;**48**:743-748. DOI: 10.1016/S1359-6462(02)00537-7

[58] Ullner C, Brauser S, Subaric-Leitis A, Weber G, Rethmeier M. Determination of local stress–strain properties of resistance spot-welded joints of advanced high-strength steels using the instrumented indentation test. Journal of Materials Science. 2012;**47**:1504-1513. DOI: 10.1007/s10853-011-5936-3

[59] Vourna P, Ktena A, Tsakiridis PE, Hristoforou E. An accurate evaluation of the residual stress of welded electrical steels with magnetic Barkhausen noise. Measurement. 2015;**71**: 31-45. DOI: 10.1016/j.measurement.2015.04.007

[60] Vourna P, Ktena A, Tsakiridis PE, Hristoforou E. A novel approach of accurately evaluating residual stress and microstructure of welded electrical steels. NDT&E International. 2015;**71**:33-42. DOI: 10.1016/j.ndteint.2014.09.011

[61] Vourna P. An accurate method for determining residual stresses with magnetic non-destructive techniques in welded ferromagnetic steels. Materials Science and Engineering. 2016;**108**:1-5. DOI: 10.1088/1757-899X/108/1/012017

[62] Ju J-B, Lee J-S, Jang J-I, Kim W-S, Kwon D. Determination of welding residual stress distribution in API X65 pipeline using a modified magnetic Barkhausen noise method. International Journal of Pressure Vessels and Piping. 2003;**80**:641-646. DOI: 10.1016/S0308-0161(03)00131-5

[63] Yelbay HI, Cam I, Gür CH. Non-destructive determination of residual stress state in steel weldments by magnetic Barkhausen noise technique. NDT&E International. 2010;**43**:29-33. DOI: 10.1016/j.ndteint.2009.08.003

[64] Stewart DM, Stevens KJ, Kaiser AB. Magnetic Barkhausen noise analysis of stress in steel. Current Applied Physics. 2004;**4**:308-311. DOI: 10.1016/j.cap.2003.11.035

[65] Gauthier J, Krause TW, Atherton DL. Measurement of residual stress in steel using the magnetic Barkhausen noise technique. NDT&E International. 1998;**31**:23-31. DOI: 10.1016/S0963-8695(97)00023-6

[66] Mitra A, Chen ZJ, Jiles DC. Nondestructive magnetic measurements in weld and base metals of service exposed Cr-Mo steel. NDT&E International. 1995;**28**:29-33. DOI: 10.1016/0963-8695(94)00002-2

[67] Lachmann C, Nitschke-Pagel T, Wohlfahrt H. Characterisation of residual stress relaxation in fatigue loaded welded joints by X-ray diffraction and Barkhausen noise method. Materials Science Forum. 2000;**347–349**:374-381. DOI: 10.4028/www.scientific.net/ MSF.347-349.374

[68] Palanichamy P, Vasudevan M, Jayakumar T. Measurement of residual stresses in austenitic stainless steel weld joints using ultrasonic technique. Science and Technology of Welding & Joining. 2009;**14**:166-171. DOI: 10.1179/136217108X394753

[69] Lu H, Liu XS, Yang JG, Zhang SP, Fang HY. Ultrasonic stress evaluation on welded plates with Lcr wave. Science and Technology of Welding & Joining. 2008;**13**:70-74. DOI: 10.1179/174329307X249405

[70] Egle DM, Bray DE. Measurement of acoustoelastic and third-order elastic constants for rail steel. The Journal of the Acoustical Society of America. 1976;**60**:741-744. DOI: 10.1121/1.381146

[71] Uzuna F, Bilge AN. Immersion ultrasonic technique for investigation of total welding residual stress. Procedia Engineering. 2011;**10**:3098-3103. DOI: 10.1016/j.proeng.2011.04.513

[72] Tanala E, Bourse G, Fremiot M, De Belleval JF. Determination of near surface residual stresses on welded joints using ultrasonic methods. NDT&E International. 1995;**28**:83-88. DOI: 10.1016/0963-8695(94)00013-A

[73] Woo W, Em V, Mikula P, An G-B, Seong B-S. Neutron diffraction measurements of residual stresses in a 50 mm thick weld. Materials Science and Engineering A. 2011;**528**: 4120-4124. DOI: 10.1016/j.msea.2011.02.009

[74] Warren BE, Averbach BL. The effect of cold-work distortion on X-ray patterns. Journal of Applied Physics. 1950;**21**:595-599. DOI: 10.1063/1.1699713

[75] Kromm A, Kannengiesser Th, Gibmeier J, Genzel Ch, van der Mee V. Determination of residual stresses in low transformation temperature (LTT-) weld metals using X-ray and high energy synchrotron radiation. Welding in the World. 2009;**53**:3-16. DOI: 10.1007/BF03266687

[76] Cheng X, Fisher JW, Prask HJ, Gnäupel-Herold T, Yen BT, Roy S. Residual stress modification by post-weld treatment and its beneficial effect on fatigue strength of welded structures. International Journal of Fatigue. 2003;**25**:1259-1269. DOI: 10.1016/j.ijfatigue.2003.08.020

[77] Monin VI, Gurova T, Castello X, Estefen SF. Analysis of residual stress state in welded steel plates by X-ray diffraction method. Reviews on Advanced Materials Science. 2009; **19**:172-175

[78] Reynolds AP, Tang W, Gnaupel-Herold T, Prask H. Structure, properties, and residual stress of 304L stainless steel friction stir welds. Scripta Materialia. 2003;**48**:1289-1294. DOI: 10.1016/S1359-6462(03)00024-1

[79] Gou R, Zhang Y, Xu X, Sun L, Yang Y. Residual stress measurement of new and in-service X70 pipelines by X-ray diffraction method. NDT&E International. 2011;**44**:387-393. DOI: 10.1016/j.ndteint.2011.03.003

[80] Paradowska AM, Price JWH, Finlayson TR, Lienert U, Walls P, Ibrahim R. Residual stress distribution in steel butt welds measured using neutron and synchrotron diffraction. Journal of Physics: Condensed Matter. 2009;**21**:1-5. DOI: 10.1088/0953-8984/21/12/124213

[81] Park MJ, Yang HN, Jang DY, Kim JS, Jin TE. Residual stress measurement on welded specimen by neutron diffraction. Journal of Materials Processing Technology. 2004;**155–156**: 1171-1177. DOI: 10.1016/j.jmatprotec.2004.04.393

[82] Albertini G, Bruno G, Dunn BD, Fiori F, Reimers W, Wright JS. Comparative neutron and X-ray residual stress measurements on al-2219 welded plate. Materials Science and Engineering A. 1997;**224**:157-165. DOI: 10.1016/S0921-5093(96)10546-3

[83] Ganguly S, Fitzpatrick ME, Edwards L. Use of neutron and synchrotron X-ray diffraction for evaluation of residual stresses in a 2024-T351 Aluminum alloy variable-polarity plasma-arc weld. Metallurgical and Materials Transactions A. 2006;**37A**:411-420. DOI: 10.1007/s11661-006-0012-3

[84] Tra TH, Okazaki M, Suzuki K. Fatigue crack propagation behavior in friction stir welding of AA6063-T5: Roles of residual stress and microstructure. International Journal of Fatigue. 2012;**43**:23-29. DOI: 10.1016/j.ijfatigue.2012.02.003

[85] Owen RA, Preston RV, Withers PJ, Shercliff HR, Webster PJ. Neutron and synchrotron measurements of residual strain in TIG welded aluminium alloy 2024. Materials Science and Engineering A. 2003;**346**:159-167. DOI: 10.1016/S0921-5093(02)00547-6

[86] Woo W, Feng Z, Wang X-L, Brown DW, Clausen B, An K, Choo H, Hubbard CR, David SA. In situ neutron diffraction measurements of temperature and stresses during friction stir welding of 6061-T6 aluminium alloy. Science and Technology of Welding & Joining. 2007; **12**:298-303. DOI: 10.1179/174329307X197548

[87] Staron P, Koçak M, Williams S, Wescott A. Residual stress in friction stir-welded Al sheets. Physica B: Condensed Matter. 2004;**350**:e491-e493. DOI: 10.1016/j.physb.2004.03.128

[88] Daymond MR, Bonner NW. Measurement of strain in a titanium linear friction weld by neutron diffraction. Physica B: Condensed Matter. 2003;**325**:130-137. DOI: 10.1016/S0921-4526(02)01514-4

[89] Turner R, Ward RM, March R, Reed RC. The magnitude and origin of residual stress in Ti-6Al-4V linear friction welds: An investigation by validated numerical Modeling. Metallurgical and Materials Transactions B. 2012;**43B**:186-197. DOI: 10.1007/s11663-011-9563-9

[90] Withers PJ. Mapping residual and internal stress in materials by neutron diffraction. Comptes Rendus Physique. 2007;**8**:806-820. DOI: 10.1016/j.crhy.2007.09.015

[91] Barbieri G, Soltani P, Kaciulis S, Montanari R, Varone A. IN792 DS superalloy: Optimization of EB welding and post-welding heat treatments. Materials Science Forum. 2016;**879**: 175-180. DOI: 10.4028/www.scientific.net/MSF.879.175

[92] Montanari R, Varone A, Barbieri G, Soltani P, Mezzi A, Kaciulis S. Welding of IN792 DS superalloy by electron beam. Surface and Interface Analysis. 2016;**48**:483-487. DOI: 10. 1002/sia.5946

[93] Angella G, Barbieri G, Donnini R, Montanari R, Richetta M, Varone A. Electron beam welding of IN792 DS: Effects of pass speed and PWHT on microstructure and hardness. Materials. 2017;**10**:1-19. DOI: 10.3390/ma10091033

[94] Montanari R, Riccardi B, Volterri R, Bertamini L. Characterisation of plasma sprayed W-coatings on a CuCrZr alloy for nuclear fusion reactor applications. Materials Letters. 2002;**52**:100-105. DOI: 10.1016/S0167-577X(01)00375-5

[95] Riccardi B, Montanari R, Casadei M, Costanza G, Filacchioni G, Moriani A. Optimisation and characterisation of tungsten thick coatings on copper based alloy substrates. Journal of Nuclear Materials. 2006;**352**:29-35. DOI: 10.1016/j.jnucmat.2006.02